Tomas GOTTHANS[1,2], Jiri PETRZELA[1]
Department of Radio Electronics, Brno University of Technology (1)
ESYCOM, ESIEE Paris, Université Paris-Est (2)

Analysis and implementation of dynamical system with periodical discrete jumps

Abstract. *The novel method for dynamical motion quantification is discussed in this paper. The proposed approach is verified on the cyclically symmetrical vector field with jump functions generating the large state space attractors recently discovered by the authors. The core part of the calculation engine involves continuous Fourier transform and Cartesian to spherical conversion. It turns out that the existing methods give the incorrect results, have huge demands on the computer performance or completely fail to converge in the finite time. The fully analog as well as hybrid circuitry implementation using off-the-shelf components is also presented and validated by means of the network simulator Orcad Pspice.*

Streszczenie. *W artykule opisano nową metodę dynamicznego kwantowania ruchu. Zasadniczą część obliczeń stanowi transformata Fouriera i sferyczna konwersja Kartezjańska. Założenia potwierdzają symulacje Pspice.* ***(Analiza i zastosowanie systemu dynamicznego z periodycznymi skokami dyskretnymi)***

Keywords: analog oscillator, dynamical system, motion quantification, chaos, state attractor, Lyapunov exponents
Słowa kluczowe: dynamiczny system kwantowania ruchu, chaos, generator analogowy

Introduction

Recently, discovery of a new interesting dynamical system has been reported by the authors and its practical implementation as an electronic circuit has been already verified [1]. This system so-called Gotthans-Petrzela(GP)[1] can be expressed by the following set of the dimensionless differential equations

$$\begin{aligned} \dot{x} &= -a_x\, x \pm sgn[\sin(b_y y)] \\ \dot{y} &= -a_y\, y \pm sgn[\sin(b_z z)] \\ \dot{z} &= -a_z\, z \pm sgn[\sin(b_x x)], \end{aligned} \tag{1}$$

where dots denote the derivatives with respect to time and the dissipative constants $-a_x \leq 0$, $-a_y \leq 0$, $-a_z \leq 0$. The constants $b_x > 0$, $b_y > 0$, $b_z > 0$ are called complexity parameters. Note that it is a modified mathematical model known as a generator of the so-called labyrinth chaos [2], has a cyclically symmetrical vector field and is invariant under the trivial changes of the state variables. It eventually turns out that sine function can be directly replaced by cosine function without the essential changes of the global dynamics. The main difference between (1) and original dynamical system describing auto-catalytic processes in chemistry is the discontinuity of the vector field. Since there is no closed-form analytic solution of the equations (1) the analysis is restricted to the numerical integration process and the associated routines. The most widely used and general quantifier of the dynamical motion is a calculation of some metric dimension of the state space attractor. First such method known as Kaplan-Yorke dimension is based on the knowledge of a spectrum of the Lyapunov exponents (LE), i.e. three real numbers which measure the average ratio of the state space volume segment expansion or contraction. The definition formula can be written as [3]

$$LE[\mathbf{x}_0, \mathbf{y}_0 \in T_{x(t)}\Re^3] = \lim_{t\to\infty} \frac{1}{t} \frac{\|D_x\phi(t,\mathbf{x}_0)\mathbf{y}_0|}{\|\mathbf{y}_0\|}, \tag{2}$$

where $T_{x(t)}$ represents a tangent space in the fiducial point and $D_x\phi(t,\mathbf{x}_0)\mathbf{y}_0$ is a solution of the linearized system. By sorting and indexing LEs in descending order the mentioned metric dimension can be calculated as

$$D_{KY} = k + \frac{\sum_{i=1}^{k} LE_i}{\|LE_{k+1}\|}, \tag{3}$$

where k is the largest integer for which the numerator in (3) is still a positive number. This formula is in accordance with two fundamental mechanisms of chaos generation, i.e. folding and stretching of the state space trajectories. From definition of the dissipative systems the sum of all LEs is negative. It is obvious from (2) that the most common approach for LE evaluation for three dimensional original systems is based on the numerical integration of the twelve differential equations [4]. The linearization matrix is calculated in each point on the trajectory, thus it necessary to have the knowledge about Jacobi matrix (JM) in the symbolic form. This method cannot be used if the vector field is discontinuous, especially if the repeated jump functions are involved in the mathematical model, since JM contains extreme values. These values are both infinity (positive as well as negative) and zero. If the transition between two states of the sign function is omitted the standard procedure returns the incorrect results. It is because the linearized flow is uniquely determined by three real negative eigenvalues and form stable node local geometry near the fiducial point. Having this configuration each edge of the volume cube shrinks suggesting that the system possess three negative LEs. In practice the transition event is not neglected and the corresponding derivative depends on the numerical integration step size. If the extreme values substituted into the Jacobi matrix the entire procedure tend to diverge and fail.

Using the concept of the box-counting method the capacity dimension can be established using the formula

$$D_C = \lim_{\varepsilon\to\infty} \frac{N(\varepsilon)}{\ln(\frac{1}{\varepsilon})}. \tag{4}$$

This method can not be considered as accurate and precise since these features strongly depend on the chosen size of the volume cubes, which is necessary to be as small as possible. Decreasing edges lead to the necessity of using a huge number of the cubes and subsequently to the large demands on the personal computer performance, especially accessible memory. It is worth nothing that this is very time consuming approach. Moreover there is a probability that several points on the state space orbit fall into one volume cube and some information about attractor geometry is lost. This drawback is partially solved by other calculation techniques involving probabilities like dimension spectrum and its derivatives, information [5] and correlation dimensions [6].

Thus this method can not be effectively used for the dynamical systems with the large state space attractors. To end the discussion about suitable method for our purpose there are still some possibilities to quantify dynamical motion using the knowledge of some state variables as time-domain waveforms [7]. The utilization of some method for deriving largest LE from the time series [8] is extremely sensitive to the routine parameters and ideologically wrong.

The above mentioned problems are the main reasons for the discovery of the novel method for metric dimension calculation. Two principles for evaluation of JM in the symbolical form will be addressed in the next chapter. Fourth chapter brings some information about the concept of new rough quantifier of the dynamical motion different from the conventional metric dimensions together with some practical examples. Fifth chapter will discuss the possibilities to model GP system by using lumped analog and mixed electronic circuits. The experimental verification via the oscilloscope screen-shots is also presented. The last chapter covers some perspectives for future work and opens the virtual space for solving the residual problems.

Numerical analysis

To obtain a brief insight into the global dynamics of equations (1) the numerical integration has been performed. To do this program Mathcad and build-in fourth-order Runge-Kutta method has been used with final time $t_m = 1000$ and time step $t_\Delta = 0.1$. The initial conditions were chosen to be $x_0 = (0.100)^T$ and the results are given in Fig. 1, Fig. 2, Fig. 3, Fig. 4, Fig. 5 and Fig. 6 as the three-dimensional perspective views. Rough approximation of the sign function means that only two harmonics are used in Fourier series. On the contrary, five harmonics are taken into account for soft approximation of sign function. Obviously there are no significant changes in the global dynamics or attractor shape. Note that for small values of ax, ay and az the corresponding state attractors is bounded in very large state space volume. The major property of chaotic solution is its extreme sensitivity to the changes of the initial conditions. This is demonstrated by a time dependence of the absolute error of the selected state variable. The initial conditions for reference system have been slightly different $x_1 = (0.10100)^T$. The exponential divergence of both state trajectories is visible in Fig. 7 and Fig. 8. A very useful tool for brief dynamical system analysis is the so-called Poincaré sections. These state space subsets allow reducing the order of studied system by one. In the case of three state variables the flow is reduced to the map on the plane, see Fig. 9, Fig. 10 and Fig. 11. For each simulation in this chapter the complexity parameters were$b_x = b_y = b_z = 10$.

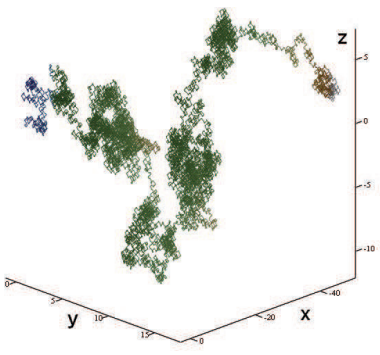

Fig. 1. Typical attractors of GP system with uniform parameters $a_x = a_y = a_z = 0$.

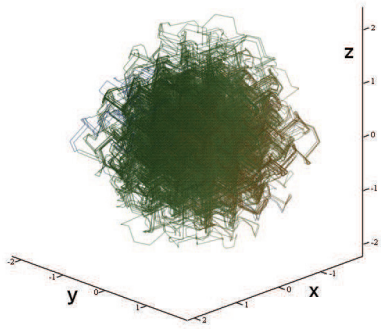

Fig. 2. Typical attractors of GP system with uniform parameters $a_x = a_y = a_z = 0.3$.

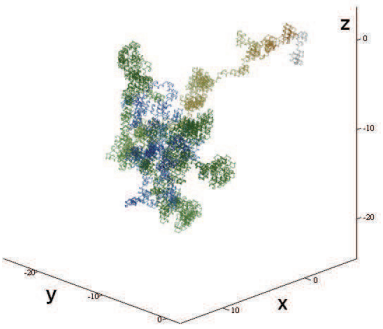

Fig. 3. Typical attractors of GP system with rough approximation of the sign function (see text) and uniform parameters $a_x = a_y = a_z = 0$.

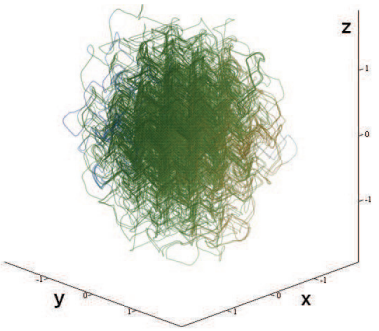

Fig. 4. Typical attractors of GP system with rough approximation of the sign function (see text) and uniform parameters $a_x = a_y = a_z = 0.3$.

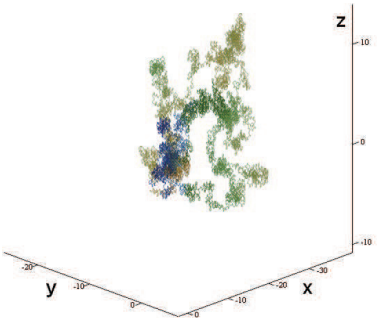

Fig. 5. Typical attractors of GP system with soft approximation of the sign function (see text) and uniform parameters $a_x = a_y = a_z = 0$.

Calculation methods

As mentioned in the first chapter the key problem of system (1) quantification is in the symbolical form of the JM. The sign function can be split into segments with zero partial derivative A_0 and regions with positive infinity $+A_\infty$ and negative infinity partial derivative $-A_\infty$. The associated characteristic polynomial becomes

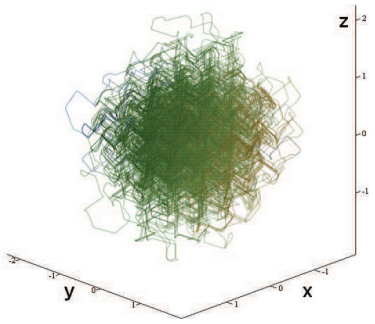

Fig. 6. Typical attractors of GP system with soft approximation of the sign function (see text) and uniform parameters $a_x = a_y = a_z = 0.3$.

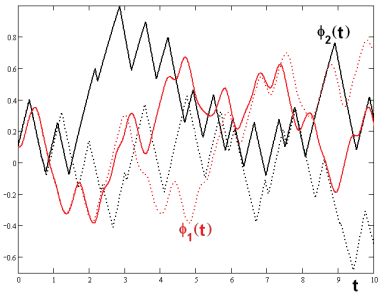

Fig. 7. Sensitivity to the changes of the initial conditions for original Thomas system (red curve) and GP system (black flow) and uniform parameters $a_x = a_y = a_z = 0$.

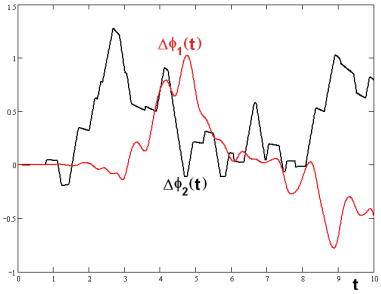

Fig. 8. Sensitivity to the changes of the initial conditions for original Thomas system (red curve) and GP system (black flow) and uniform parameters $a_x = a_y = a_z = 0.3$.

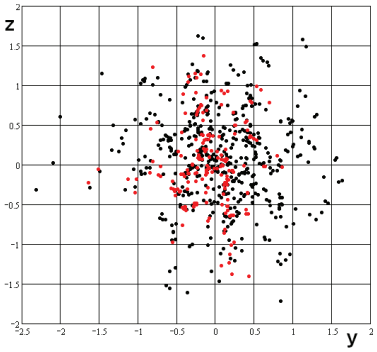

Fig. 9. Attractor visualization using different Poincaré sections corresponding to the planes $x = 0$,$y = 0$ and$z = 0$ for original Thomas system (red dots) and GP system (black dots) and uniform parameters $a_x = a_y = a_z = 0.3$.

$$\det(\lambda \cdot \mathbf{E} - \mathbf{J}) = \begin{pmatrix} \lambda - a_x & -\varphi_x & 0 \\ 0 & \lambda - a_y & -\varphi_z \\ -\varphi_x & 0 & \lambda - a_z \end{pmatrix} = (\lambda - a_x)(\lambda - a_y)(\lambda - a_z) - \varphi_x\varphi_y\varphi_z = 0, \tag{5}$$

where $\varphi = 0$ inside each segment of the vector field and $\varphi = \pm\infty$ on the boundaries. The idea about the individual

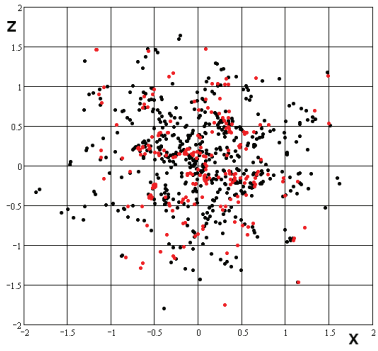

Fig. 10. Attractor visualization using different Poincaré sections corresponding to the planes $x = 0$,$y = 0$ and$z = 0$ for original Thomas system (red dots) and GP system (black dots) and uniform parameters $a_x = a_y = a_z = 0.3$.

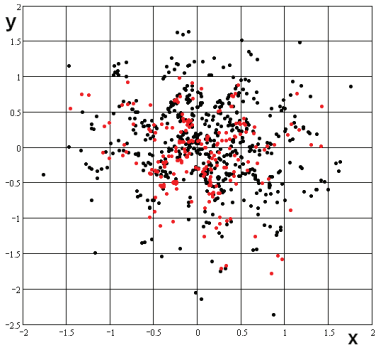

Fig. 11. Attractor visualization using different Poincaré sections corresponding to the planes $x = 0$,$y = 0$ and$z = 0$ for original Thomas system (red dots) and GP system (black dots) and uniform parameters $a_x = a_y = a_z = 0.3$.

state variables time dependence is provided in Fig. 12 and Fig. 13 for z(t). The dynamics of GP system is compared with the smooth Thomas system in the sense of third differential equation (1) which evolves accordingly to the following analytic formula (using separation of the variables)

$$\frac{dz}{dt} = a_z z + f(x) \Rightarrow z(t) = \frac{1}{a_z}[e^{a_z t} - f(x)], \tag{6}$$

where $f(x) = sign[sin(bx)]$ and $g(x) = sin(bx)$. This solution can be interpreted as increasing if $f(x) = 1$ and decreasing if $f(x) = -1$ with uniform ratio proportionally to parameter a_z. A more comprehensible image about dynamical motion governed by the last equation (1) is shown in Fig. 14 and Fig. 15. The raising and falling segments with size $k\pi/bx$ and $k\pi/bx$ where$k \in (-\infty, +\infty)$ is a natural number are also clarified in these Monge projections.

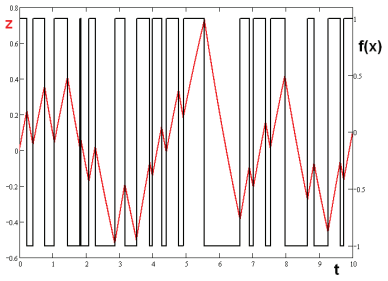

Fig. 12. The state variable z(t) waveform of GP system with uniform parameters $a_x = a_y = a_z = 0.3$.

The most straightforward approach to avoid problems with infinity is to expand the periodical sign function into the Fourier series. It is well known that the square wave, if gen-

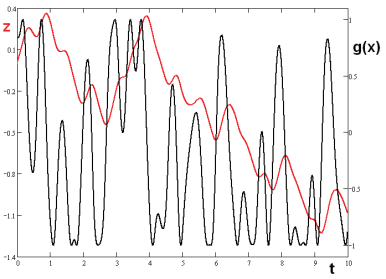

Fig. 13. The state variable z(t) waveform of Thomas system with uniform parameters $a_x = a_y = a_z = 0.3$.

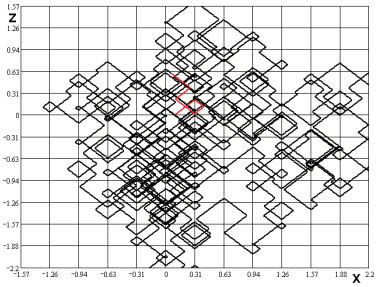

Fig. 14. The dynamical motion clarification for the last differential equation using xz plane projection, uniform parameters $a_x = a_y = a_z =$.

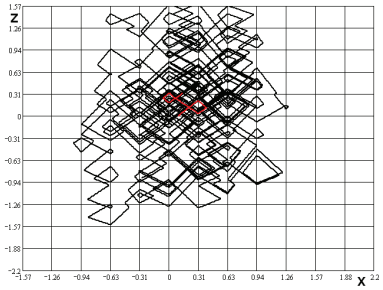

Fig. 15. The dynamical motion clarification for the last differential equation using xz plane projection, uniform parameters $a_x = a_y = a_z = 0.3$.

erated by sine function, can be expressed as

$$f(bx) = \frac{4}{\pi}\sum_{n=1}^{k}\frac{1}{2n-1}\sin[b(2n-1)x], \tag{7}$$

where k is order of the approximation. Its derivation in the symbolical form

$$g(bx) = \frac{4}{\pi}\sum_{n=1}^{k} b\sin[b(2n-1)x], \tag{8}$$

is adopted inside JM. This approach bears a significant numerical error due to the so-called Gibbs effect [10]. Intuitively speaking, the magnitude of such error depends on the integration step size. Gibbs effect introduces the fiction of the short-time decreasing volume element expansion and contraction under the dynamical flow. There are some other smooth functions with continuous derivatives that can be utilized like exponential or sigmoid functions. It turns out that calculating the spectrum of LEs by the usage of the immediate numerical value of the derivative by storing previous values of the corresponding state variable, can not be used. Extreme values of derivatives causes divergences in computation. Changing the step of numerical integration can avoid the extreme values of derivatives, but causes deviance in the final attractor itself. The topographically scaled contour-surface plots of the largest LE as a function of $a = a_x = a_y = a_z$ and $b = b_x = b_y = b_z$ are provided in Fig.16 , Fig. 17, Fig. 18 and Fig. 19.

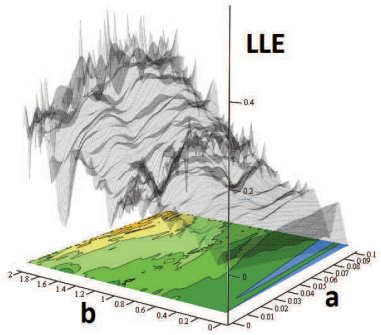

Fig. 16. Plot of the largest LE of GP system with uniform parameters $a_x = a_y = a_z \in < 0; 0.1 >$, rough approximation of the sign(.) function. In both plots $b \in < 0; 2 >$.

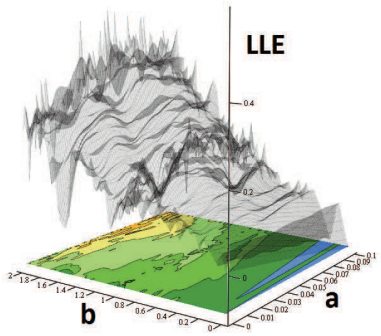

Fig. 17. Plot of the largest LE of GP system with uniform parameters $a_x = a_y = a_z \in < 0.25; 0.35 >$, rough approximation of the sign(.) function. In both plots $b \in < 0; 2 >$.

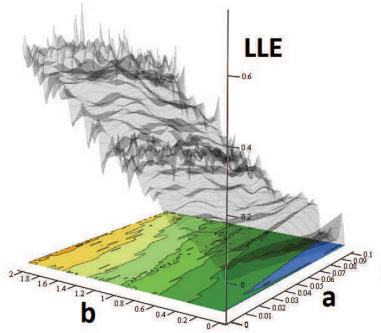

Fig. 18. Plot of the largest LE of GP system with uniform parameters $a_x = a_y = a_z \in < 0; 0.1 >$ (left), smooth approximation of the sign(.) function. In both plots $b \in < 0; 2 >$.

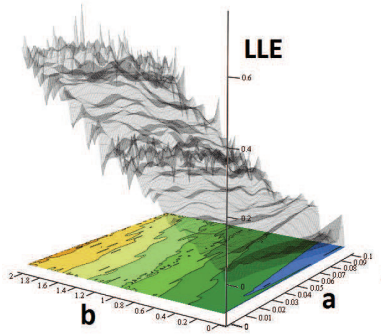

Fig. 19. Plot of the largest LE of GP system with uniform parameters $a_x = a_y = a_z \in < 0.25; 0.35 >$, smooth approximation of the sign(.) function. In both plots $b \in < 0; 2 >$.

Spherical quantification

By referring to the best knowledge of the authors there is a lack of suitable methods for quantifying behavior of almost conservative systems with large strange attractors. Thus it is time to leave metric dimensions and develop a little bit different quantifier. The proposed approach is based on the fundamental nature of the strange attractors, namely its ergodicity and mixing property. To greatly shorten the computational time the three-body problem should be exchanged by the mathematical operations on the plane, in detail on the surface of the sphere. The principle of calculation lies in the transformation of the analyzed attractor from the Cartesian coordinates into the sphere. First the surface of R^3 sphere is normalized to have general quantifier. Using the spherical coordinates, the unit sphere can be parameterized by

$$\vec{r}(\theta,\varphi) = (\cos\varphi\sin\varphi, \sin\theta\sin\varphi, \cos\varphi), \quad \wedge\, 0 \le \theta \le 2\pi, 0 \le \varphi \le \pi. \tag{9}$$

Than the area A of sphere S is set to be equal to 1 (normalization) can be expressed as

$$A(S) = \int_S |\vec{r}_u \times \vec{r}_v| du dv = 1. \tag{10}$$

Thus for the square radius r^2 of R^3 sphere stands

$$r^2 = \frac{1}{4\pi}. \tag{11}$$

Radius of this ball is chosen $r = (4\pi)^{-1/2}$ such that the sum of all SP is unity. This globe splits into elemental surface pieces (SP) depending on the $\Delta\varphi$, $\Delta\theta$ angle steps

$$\theta = \arctan\left(\frac{y}{x}\right), \tag{12}$$

$$\varphi = \arccos\left(\frac{z}{r}\right). \tag{13}$$

Assuming attractor will fill the entire space of R^3 where integral step limit approaches zero, meaning the likelihood has a continuous uniform distribution $P(x)$ is described

$$P(x) = \begin{cases} \frac{1}{b-a} & for a \le x \le b \\ 0 & for x < a \text{ or } x > b \end{cases} \tag{14}$$

Than the surface of whole sphere can be expressed as

$$S_{Sphere} = \int_0^{\pi}\int_0^{2\pi} \frac{1}{4\pi}\sin\theta d\varphi d\theta = 1. \tag{15}$$

Considering the discrete time series, the step $\Delta\theta$ and $\Delta\varphi$ needs to be set, otherwise certain SP needs to be deleted to have particular list of SP the complexity of the analyzed attractor. Following the flow $\Phi(x,y,z)$ of attractor in R^3 of N elements, each SP is indexed by the natural numbers i and j. In the main calculation routine the individual SP occupied by a state trajectory are summarized. The surface of occupied area on the R^3 sphere can be calculated using the following discrete formula

$$S_\Phi = \sum_{i=1}^{N}\sum_{j=1}^{N} \frac{1}{4\pi}\sin(i\frac{\pi}{N})2ij\frac{\pi^2}{N^2}. \tag{16}$$

The graphical interpretation of this novel motion quantifier is demonstrated in Fig. 20, Fig. 21, Fig. 22, Fig. 23, Fig. 24 and Fig. 25 for some interesting situations. There is one serious drawback of this procedure leading to the indispensable numerical errors. The shape and orientation of the state attractor can be right-lined as it is visible in the first two examples. If so, a huge amount of the information about attractor geometric structure is lost. To improve this disadvantage the linear change of the coordinates in order to spread the studied attractor should be performed before transformation on the sphere.

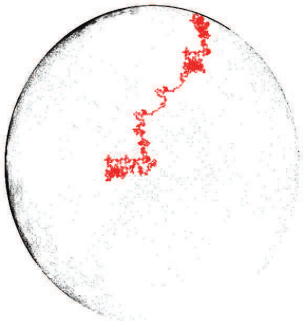

Fig. 20. The dynamical motion quantification, analyzed attractor (red) and its projection on sphere (black), GP system with uniform parameters $a_x = 0.1$ and $a_y = a_z = 0$.

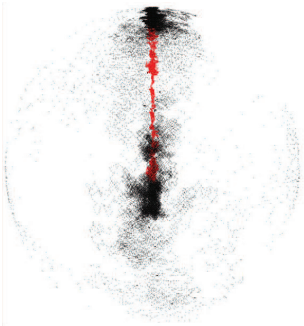

Fig. 21. Another view on the dynamical motion quantification, analyzed attractor (red) and its projection on sphere (black), GP system with uniform parameters $a_x = 0.1$ and $a_y = a_z = 0$.

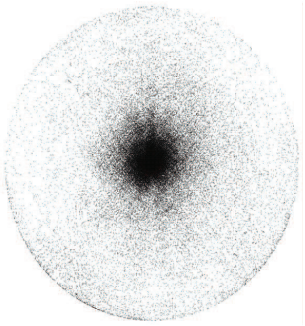

Fig. 22. The dynamical motion quantification, analyzed attractor (red) and its projection on sphere (black), GP system with uniform parameters $a_x = a_y = 0.1$ and $a_z = 0$.

Circuitry implementation

It is well known that synthesis of the electronic circuits is the easiest way how to accurately model the nonlinear dynamical systems. There are three major and widely used systematic approaches: classical circuit synthesis [1], direct implementation of the differential equation [2] and design procedure based on the integrator block schematic [3]. Each mentioned design approach has some advantages and drawbacks and it is up to the engineer to choose the correct one. The circuitry implementation of the continuous time dynamical systems with accessible chaotic behavior is called chaotic oscillator. Due to the stretching mechanism usually caused

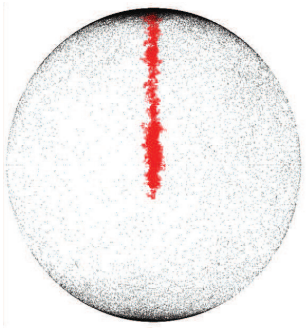

Fig. 23. Another different view on the dynamical motion quantification, analyzed attractor (red) and its projection on sphere (black), GP system with uniform parameters $a_x = a_y = 0.1$ and $a_z = 0$.

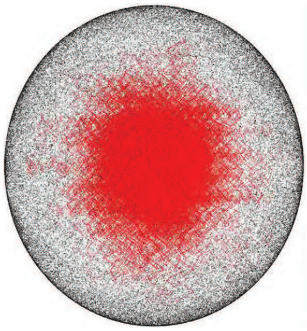

Fig. 24. The dynamical motion quantification, analyzed attractor (red) and its projection on sphere (black), GP system with uniform parameters $a_x = a_y = a_z = 0.1$.

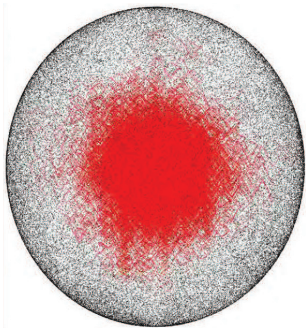

Fig. 25. Another different view on the dynamical motion quantification, analyzed attractor (red) and its projection on sphere (black), GP system with uniform parameters $a_x = a_y = a_z = 0.1$.

by single or multiple unstable equilibrium the corresponding circuit must contain one or more active elements [4] supplying energy to the passive parts. The most straightforward way for practical realization of Thomas dynamical system as well as GP oscillator starts with block schematic with inverting integrators, differential amplifiers (with summation block as a special case) and two-port with desired nonlinear transfer characteristics. One possible network suitable to model GP system is given in Fig. 1 and Fig. 2. The disadvantage of such configuration is clear: a large amount of the active building blocks. The linear part of the vector field is composed of the linear lossy integrators realized by the second generation positive current conveyor (CCII+) with current summation at the input port. CCII+, in particular the integrated circuit AD844, is described by the set of following hybrid equations

$$i_y = 0 \; u_x = u_y \; i_z = i_x \; u_0 = u_z. \tag{17}$$

The purpose of CCII+ is also for easy measurement of the nonlinear function, which is represented by voltage at the output u_0. The principle of the piecewise-constant function is fundamental. The operational amplifiers act as comparators (CMP) without hysteresis effect. The transfer function and integration can be expressed by single equation in Laplace transform

$$_0 = -\frac{1}{sC+G}\sum_{k=1}^{i}\frac{u_k}{R_{xk}}, \tag{18}$$

where $G = 1/R$, uk are voltages at the output of CMP and i is the number of necessary CMP which is closely related to the dissipation factors a_x, a_y, a_z adjustable by the variable resistors R. The size of accessible state attractor is upper limited by the dynamical ranges of the OPA, i.e. by supply voltages $V_{cc} = 15V$ and $V_{ee} = -15V$. The breakpoints of the transfer curve are adjusted either by external dc sources or voltage divider made by the resistors R_{di}.

The time-domain simulation of the fully analog GP system is shown in Fig. 3 and Fig. 4 as the plane projections of the strange state space attractors.

The main drawback of the fully analog oscillator conception is obvious, a huge number of the active elements. The idea behind digital approach is uncovered in Fig. 26. The linear part of the vector field remains the same as for previous oscillator. The input signal enters analog-to-digital converter (ADC), goes through processor programmed in C/C++ using KEIL uVision V3.90 and resulting waveform is finally transformed back into the analog form by digital-to-analog converter (DAC). The slowest operation is computing trigonometric function. The maximum working frequency is about 230 kHz and this boundary has been verified either by numerical pre-study in Mathcad (sampling and quantization mechanism) as well as by experimental measurement. The selected digital oscilloscope screen-shots are provided in Fig. 27, Fig. 28 and Fig. 29 proving almost one-to-one correspondence between the theoretical expectations and the practical results. For further questions or comments please do not hesitate to contact the authors and for more detail consult paper [15] or [1].

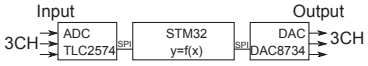

Fig. 26. Experimental setup for implementation of GP system by means of six-port with digital signal processing.

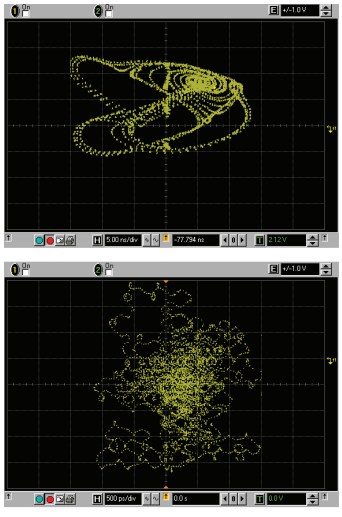

Fig. 27. Experimental verification of mixed circuit design of GP system measured by Agilent Infiniium.

After thinking about how to reduce the complexity of the nonlinear network a very simple circuitry has been revealed.

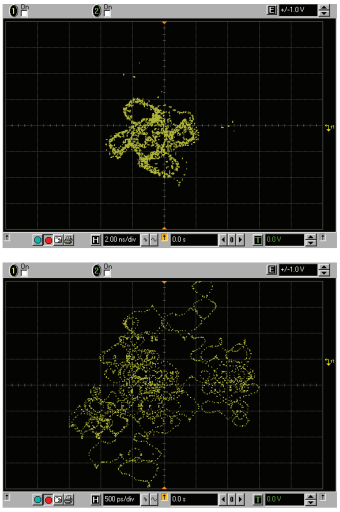

Fig. 28. Experimental verification of mixed circuit design of GP system measured by Agilent Infiniium.

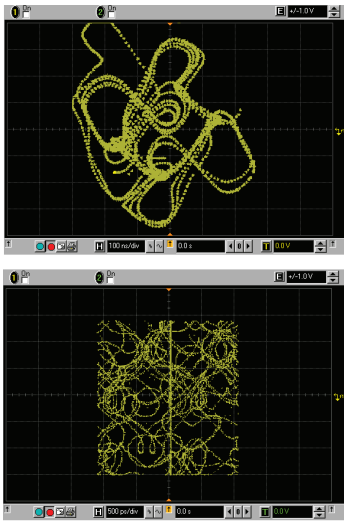

Fig. 29. Experimental verification of mixed circuit design of GP system measured by Agilent Infiniium.

The stair-type function can be realized by single ADC, namely by considering its least significant bit. Of course the input voltage range should be adjusted accordingly to the parameter b_x, b_y and b_z. The output voltage level should be also carefully monitored and shifted by negative offset voltage if necessary. The realization itself can be seen in Fig. 32 and its circuit simulations using Orcad Pspice 15 environment in Fig. 33. In this particular case, two ADC blocks were used. One for positive voltage with positive voltage reference VREF1 and other for negative VREF2. Voltage offset is added by voltage sources VOFF. But in fact, only one ADC can be used with positive and negative voltage dynamical range. Resistors $R_d \sim 1k\Omega$. The parameter b is set directly by the sampling frequency of the converter itself. Values of parameter a_x, a_y and a_z are set by resistors R_x, R_y and R_z.

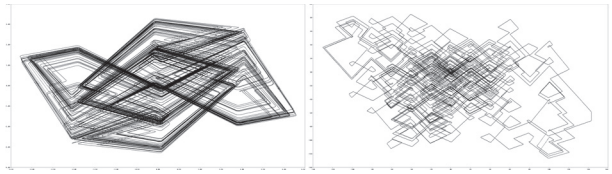

Fig. 30. The plane projections of the state space trajectories simulated in Orcad Pspice 15 environment, $b_x = b_y = b_z = 10$ together uniform dissipation parameters $a_x = a_y = a_z = 0.5$ (left) and $a_x = a_y = a_z = 0.2$ (right).

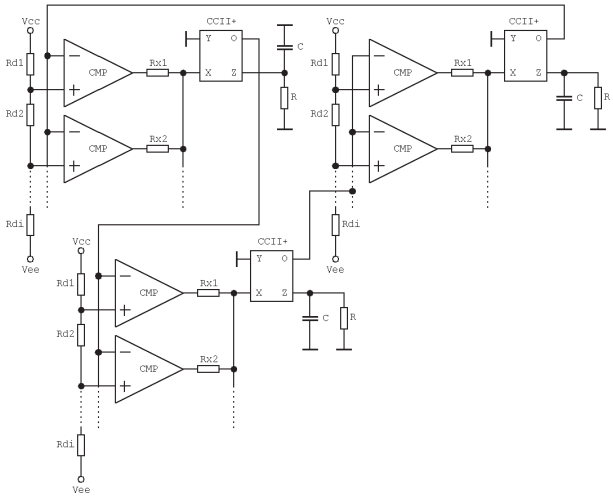

Fig. 31. Fully analog implementation of GP system using AD844 (CCII+) and TL084 (OPA).

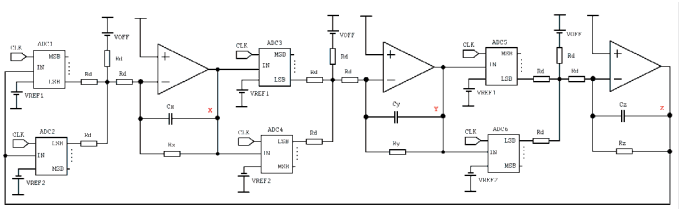

Fig. 32. GP system realization by using ADC as core engine for the nonlinear building block.

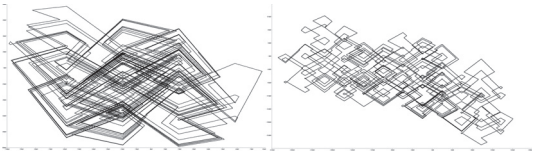

Fig. 33. The plane projections of the state space trajectories of ADC realization simulated in Orcad Pspice 15 environment, $b_x = b_y = b_z = 10$ together uniform dissipation parameters $R_x = R_y = R_z = 10k\Omega$ (left) and $R_x = R_y = R_z = 70k\Omega$ (right).

Conclusion

The several novel ideas from the area of numerical analysis of the dynamical systems with low dissipation have been suggested and verified. These procedures allow solving the serious problems where standard existing procedures can not be used. Even though the proposed generalizations are not completely finished yet and form a topic for further study, derived procedures can be utilized for various arbitrary-order systems with discontinuous dynamical flows. Moreover, the authors believe that GP oscillator models the three-dimensional Brownian motion [16] of the single microscopic particle without interactions. The vector field discontinuity and flow jumping resembles the particle-like behavior known from the quantum theory [17]. There is no doubt that there are a lot of real physical systems with the similar mathematical description. The very interesting joiner to the study of GP oscillator would be the description of stable and unstable manifolds, boundary planes and basin of attraction [9].

Acknowledgments

The research is a part of the COST action IC0803, which is supported by the Czech Ministry of Education under grant no. OC09016. The support of project CZ.1.07/2.3.00/20.0007 WICOMT, financed from the operational program Education for Competitiveness, is gratefully acknowledged. Measurements were performed in laboratories supported by the SIX project; the registration number CZ.1.05/2.1.00/03.0072, the operational program Research and Development for Innovation. Publication of the results was financially supported by the project Popularization of BUT R &D Results and Support of Systematic Collaboration with Czech Students, no.CZ.1.07/2.3.00/35.0004.

REFERENCES

[1] Petrzela, J., Gotthans, T., Hrubos, Z., Analog implementation of Gotthans-Petrzela oscillator with virtual equilibria. In Proceedings of 21st International Conference Radioelektronika 2011, Brno (Czech Republic), p. 53 – 56.

[2] Sprott, J. C., Chlouverakis, K. E. Labyrinth chaos. International Journal of Bifurcation and Chaos, 2007, vol. 17, no. 6, p. 2097 – 2108.

[3] Grygiel, K., Szlachetka, P. Lyapunov exponents analysis of autonomous and nonautonomous set of ordinary differential equations. Acta Physica Polonica B, 1995, vol. 26, no. 8, pp. 1321 – 1331.

[4] Petrzela, J. Modeling of the strange behavior in the selected nonlinear dynamical systems, part II: analysis. VUTIUM Press, 2010.

[5] Hentschell, H. G. E., Procaccia, I. The infinite number of generalized dimensions of fractals and strange attractors. Physica D, 1983, vol. 8, p. 435 – 444.

[6] Grassenberger, P., Procaccia, I. Characterization of strange attractors. Physical Review Letters, 1983, vol. 50, p. 346 – 349.

[7] Sprott, J. C., Chaos and time series analysis. Oxford University Press, 2003.

[8] Wolf, A., Swift, J. B., Swinney, H. L., Vastano, J. A. Determining Lyapunov exponents from a time series. Physica 16D, 1985, p. 285 – 317.

[9] Spany, V., Galajda, P., Guzan, M., Pivka, L., Olejar, M. Chua's singularities: great miracle in circuit theory. International Journal of Bifurcation and Chaos, 2010, vol. 20, no. 10, pp. 2993 – 3006.

[10] Barry, N. Treatise on trigonometric series. The Macmillan Company, New York, 1964.

[11] Itoh, M. Synthesis of topologically conjugate chaotic nonlinear circuits. International Journal of Bifurcation and Chaos, 1997, vol. 7, no. 6, p. 1195 – 1223.

[12] Itoh, M. Synthesis of electronic circuits for simulating nonlinear dynamics. International Journal of Bifurcation and Chaos, 2001, vol. 11, no. 3, p. 605 – 653.

[13] Petrzela, J. Modeling of the strange behavior in the selected nonlinear dynamical systems, part I: oscillators. VUTIUM Press, 2008.

[14] Biolek, D., Senani, R., Biolkova, V., Kolka, Z. Active elements for analog signal processing: classification, review and future perspectives. Radioengineering, 2008, vol. 17, no. 4, p. 15 – 32.

[15] Petrzela, J., Hrubos, Z., Gotthans, T. Modeling deterministic chaos using electronic circuits. Radioengineering, 2011, vol. 20, no. 2, p. 438 – 444.

[16] Morters, P., Peres, Y. Brownian motion. Cambridge University Press, 416 pages, 2008.

[17] Ocampo, H., Paycha, S., Reyes, A. Geometric methods for quantum theory. World Scientific, 530 pages, 2008.

***Authors**: Ing. Tomas Gotthans, Doc. Ing. Jiri Petrzela, PhD., Department of Radio Electronics, Faculty of Electrical Engineering, Brno University of Technology, Purkynova 118, 612 00 Brno, Czech Republic, email: tomas.gotthans@phd.feec.vutbr.cz,*